

# SCIENTIFIC REPORTS

OPEN

## One-step Maskless Fabrication and Optical Characterization of Silicon Surfaces with Antireflective Properties and a White Color Appearance

Received: 21 June 2016  
Accepted: 27 September 2016  
Published: 11 October 2016

Ling Schneider<sup>1</sup>, Nikolaj A. Feidenhans<sup>1,2</sup>, Agnieszka Telecka<sup>1</sup> & Rafael J. Taboryski<sup>1</sup>

**We report a simple one-step maskless fabrication of inverted pyramids on silicon wafers by reactive ion etching. The fabricated surface structures exhibit excellent anti-reflective properties: The total reflectance of the nano inverted pyramids fabricated by our method can be as low as 12% without any anti-reflective layers, and down to only 0.33% with a silicon nitride coating. The results from angle resolved scattering measurements indicate that the existence of triple reflections is responsible for the reduced reflectance. The surfaces with the nano inverted pyramids also exhibit a distinct milky white color.**

Silicon is abundant in nature, and has been widely used in the semiconductor industry. By texturing silicon surfaces, it is possible to obtain samples of dual- or multi-functions that are attractive in many fields. Recently, there has been increasing interest in using “black silicon” fabricated by reactive ion etching (RIE) to enhance the light trapping efficiency of photovoltaic devices<sup>1–6</sup>. The RIE fabricated silicon typically consists of needle-like or cone-shape structures that scatter the incident light, which is the reason for the black or brownish color of the surface<sup>3,7–11</sup>. Though highly anti-reflective, the black silicon suffers from high surface recombination losses caused by its extremely high surface area, which as a result limits the increase of the external quantum efficiency of photovoltaic devices<sup>12,13</sup>. Recently, Savin *et al.* reported that it is possible to chemically and electrically passivate the black silicon to reduce the charge recombination by depositing an alumina layer<sup>14</sup>. Alternatively, it has been reported that inverted pyramids have lower surface areas than upright pyramids, yet still good light trapping properties<sup>12,13,15–20</sup>. These inverted pyramids are typically fabricated either by colloidal lithography<sup>21,22</sup>, or by combining interference lithography and wet silicon etching<sup>13,16,17,19</sup>. Both methods are complex and require masks or templates for the fabrication, which increases the fabrication costs. Wang *et al.* recently reported on using a maskless copper assisted acid etching method to fabricate micro inverted pyramids on a silicon surface<sup>20</sup>. Nonetheless, as copper is a deep donor for silicon, the use of copper could potentially cause contamination to the fabricated samples and other processes performed in the same cleanroom.

In this letter we report a simple one step maskless method to fabricate semi-periodic nano inverted pyramids on silicon wafer surfaces by RIE. RIE is a dry etching technique that can be used to structure silicon surfaces through the combined effect of a corrosive gas ( $\text{SF}_6$  or  $\text{CH}_4$ ) and a passivating gas ( $\text{O}_2$ ) without additional masks<sup>7,8</sup>. We will show that by fine tuning the etching parameters, we are able to fabricate nano inverted pyramids of different sizes and regularities. The total reflectance of the inverted pyramids fabricated by our method can be as low as 12% without any anti-reflective layers, and down to only 0.33% with silicon nitride ( $\text{SiN}_x$ ) coatings. The surfaces with the uncoated nano inverted pyramids also exhibit a very interesting milky white color, which to the best of our knowledge has not been reported yet. As reactive ion etching (RIE) is widely used in the semi-conducting industry, our technique will have high potential not only in the photovoltaic but also other

<sup>1</sup>Department of Micro- and Nanotechnology, Technical University of Denmark, 2800 Kongens Lyngby, Denmark.

<sup>2</sup>Danish Fundamental Metrology A/S, Matematiktorvet 307, 2800 Kongens Lyngby, Denmark. Correspondence and requests for materials should be addressed to L.S. (email: lisu@nanotech.dtu.dk) or R.J.T. (email: rata@nanotech.dtu.dk)

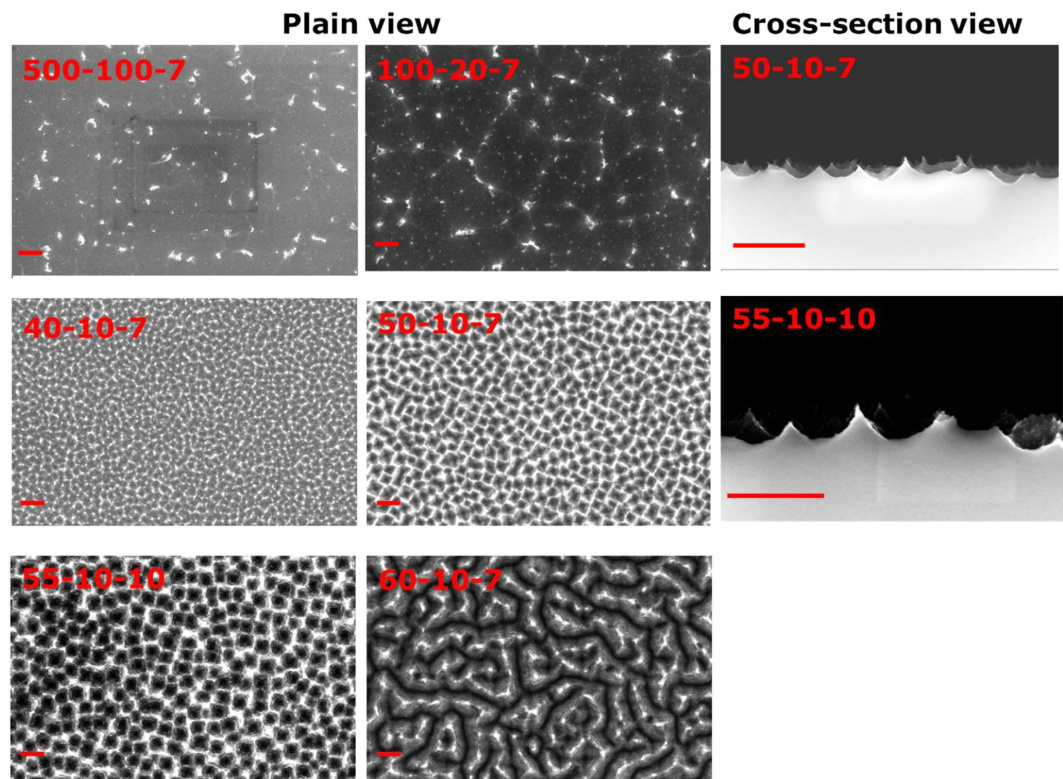


**Figure 1.** SEM images of structures fabricated at different gas flow rates and etching times. The scale bars are 1  $\mu\text{m}$ .

industries, where surfaces of special optical properties are desired. Moreover, this technique will lead towards cost-effective large-scale productions of inverted pyramidal structures.

The structure fabricated by RIE is determined by complex reactions happening inside the RIE chamber, which according to many studies depend mainly on the gas ratio, chamber temperature, chamber pressure, and the platen power<sup>2,3,5,10,11,23–26</sup>. The absolute gas flow on the other hand does not seem to have much influence on the formed structures. However, in most of the aforementioned studies, the change of the gas flow rate is only within 10%, which perhaps is too small to influence the structure formation. To better understand the parameter influence and better control the etched structures, in this study we fixed the chamber temperature ( $-19^\circ\text{C}$ ), chamber pressure (38 mTorr), and the platen power (6 W), and varied the flow rates  $Q$  (in sccm) of  $\text{SF}_6$  and  $\text{O}_2$  and the etching time  $t$  (in min). The total gas flow rate can be 12 times higher for the batches with the highest rate than for those with the lowest rate. For simplification, we denote our samples of different etching parameters as  $Q_{\text{SF}_6} - Q_{\text{O}_2} - t$ .

By changing the  $\text{SF}_6$  and  $\text{O}_2$  flow rates and the etching time, we are able to obtain wafer-scale samples of very different surface structures with good reproducibility (samples 55-10-10, 50-10-15, and 50-10-20 were reproduced five times), as presented in Fig. 1. The fabricated structures range from flat surfaces with random particles (500-100-7 and 100-20-7), winding micro-trenches (60-10-7), non-periodic holes (40-10-7), to semi-periodic inverted pyramids (50-10-7 and 55-10-10). It is worth mentioning that the gas ratio  $Q_{\text{SF}_6} : Q_{\text{O}_2}$  and the etching time  $t$  of samples 500-100-7 and 50-10-7 are the same, while the resulting structures of the two samples are very different: the surface of sample 500-100-7 is almost flat with only some random particles of irregular shape; while the surface of sample 50-10-7 already has inverted pyramidal holes. Apparently, in our study the influence of the total flow rate on the structure formation can be substantial. The dominant effect seems to be the residence time of the gas molecules in the active etching zone, where the plasma is generated. The average residence time  $\tau$  of a gas inside the RIE chamber can be defined as:  $\tau = pV/Q^{2.5}$ , where  $p$  is the pressure inside the chamber,  $V$  the plasma volume, and  $Q$  the gas flow rate. As we used fixed chamber pressures in all experiments, the throttle valve opened more for higher gas flow rates to maintain the chamber pressure than the lower ones. For a comparison, the average gas residence time of sample 500-100-7 is only 0.02 s (Fig. S2), while  $\tau$  of sample 50-10-7 is 0.21 s. Hence, for the high gas flow rates, gases pass the active etching zone so fast that there is not enough time for them to dissociate and react with the sample surface in the chamber, leading to an almost flat surface (sample 500-100-7). Similar observations were also reported by Jansen *et al.*<sup>26</sup>.

Figure 2b,c are representative spectra of the specular and total reflectance of all fabricated types. Three samples with inverted pyramidal structures (50-10-15, 50-10-20, and 55-10-10) are among those of the lowest specular and total reflectance (Fig. 2a,b). The total reflectance of sample 55-10-10 (without anti-reflective coating) is lower than 20% at shorter wavelength, and as low as 12% at near IR, which is lower than many reported values of uncoated nano/micro inverted pyramids made by more complex methods<sup>17,27,28</sup>. The inverted pyramids of this sample (55-10-10) are almost arranged in a hexagonal array, and yet with a predominantly quadratic base having

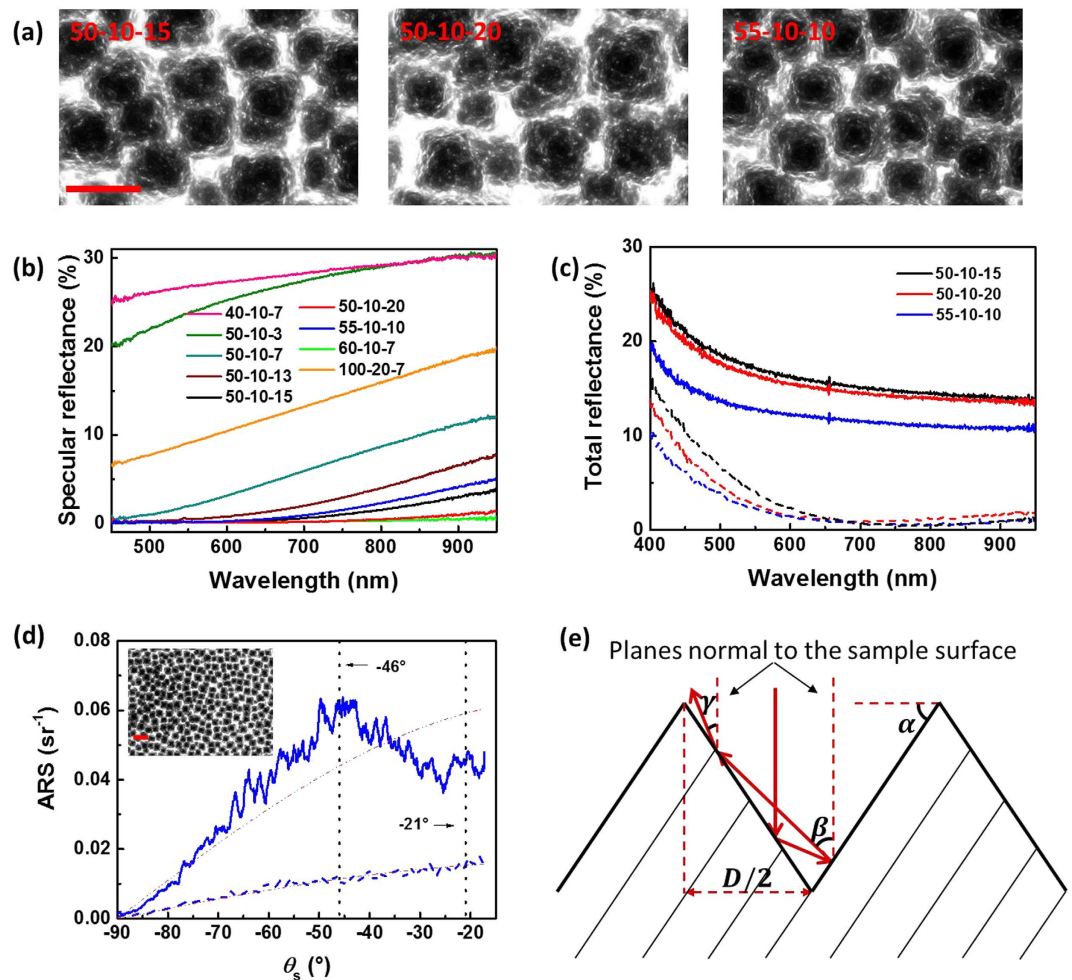


**Figure 2.** (a) SEM images of uncoated inverted pyramids. (b) Specular reflectance of uncoated samples measured at normal incidence. (c) Total reflectance of inverted pyramids without (solid line) and with (dash line)  $\sim 80$  nm  $\text{SiN}_x$  coating measured with an integrating sphere. (d) Angle resolved scattering (ARS) spectra of sample 55-10-10 without (blue solid line) and with (blue dash line)  $\text{SiN}_x$  coating measured by a diode laser of 488 nm. The red dash-dot lines are cosine fittings of the corresponding ARS curves. Inset: SEM image of uncoated 55-10-10. (e) Sketch of possible reflections of the incident light beam by one inverted pyramid. The scale bars are  $1\ \mu\text{m}$ .

side lengths of around 600 nm and a pitch distance of around 700 nm, much smaller than those reported by Wang *et al.*<sup>20</sup>. The total reflection of these three samples is further reduced down to only 0.33% after coating with the anti-reflective layer ( $\sim 80$  nm, Fig. 2c), which is also used as a passivation layer to reduce the surface recombination rate and to increase the effective carrier lifetime in photovoltaic devices<sup>13,29,30</sup>.

Figure 2d shows the angle resolved scattering (ARS) spectra of sample 55-10-10 without and with  $\text{SiN}_x$  coating. The solid-dash lines are the respective cosine fittings of the scattered intensity at angle  $\theta_s$ ,  $\text{ARS} = A \cdot \cos(\theta_s)$ . Here  $A$  is a prefactor, and  $\theta_s$  is the angle between the detector and the plane normal to the sample surface (sample normal). The ARS curve of the uncoated 55-10-10 fits well at large angles but deviates from the cosine function at small angles. There are two peaks at  $\theta_s \approx -46^\circ$  and  $\theta_s \approx -21^\circ$ , which could result from double and triple reflections of incoming beam rays by the facets of the inverted pyramids, as illustrated in Fig. 2e. The average plane inclination of the inverted pyramids is  $\alpha \approx 56.5^\circ$ , as measured by ImageJ on SEM images. This angle is close to the well-known angle of  $54.7^\circ$  usually obtained for anisotropic wet etching of  $\langle 100 \rangle$  Si surfaces with potassium hydroxide (KOH). By simple trigonometry, the angle of the second reflection to the sample normal can be derived  $\beta \approx 46^\circ$ , and the angle of the third reflection to the sample normal  $\gamma \approx 21^\circ$ . The values of these two angles fit well with the positions of the two peaks observed in Fig. 2d. The intensity difference between the two peaks can have two origins: 1. The reflection fraction of flat silicon surfaces varies at different angles of incidence according to the Fresnel equation; 2. For an inverted pyramid of  $D \approx 609$  nm and  $\alpha \approx 56.5^\circ$  as presented in Fig. 2e, only 15% of the incoming beam (per facet) falls in an area, where a third reflection could happen; the rest would be either reflected out of the inverted pyramid or absorbed by the pyramid (refracted). Similar hypothesis of triple reflections of inverted pyramids was also suggested by other groups<sup>17,20</sup>. Due to the restriction of our experimental setup, light scattered to angles lower than  $17^\circ$  to the sample normal could not be measured, which makes it

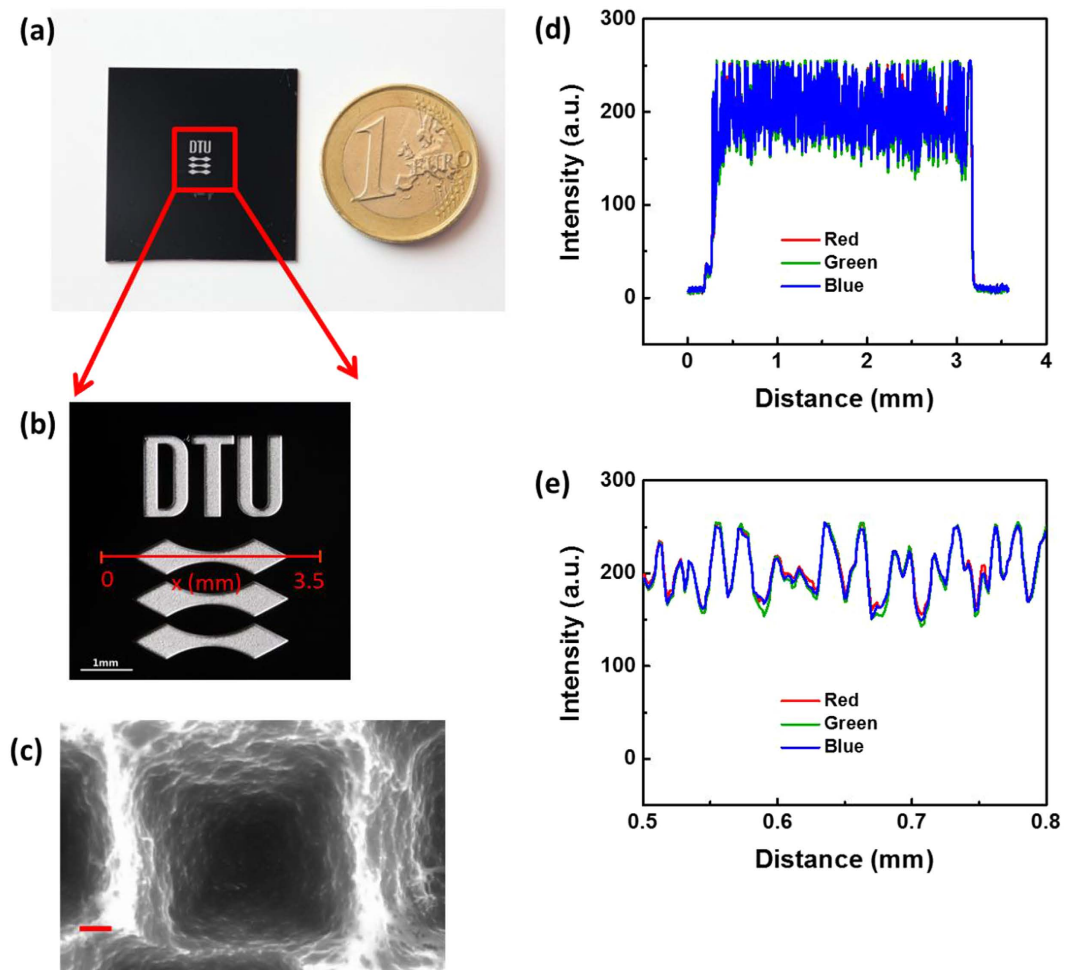


**Figure 3.** (a) Photo of a black silicon wafer with the as fabricated white DTU logo, in reference to a one EUR coin. Both the wafer and the coin were placed on a white A4 paper for color reference. (b) The zoomed photo of the logo area. (c) SEM image of one single inverted pyramid in the DTU logo area. The scale bar is 200 nm. (d) The intensity profile of RGB colors (red, green, and blue) along the red line indicated on (b). (e) The zoomed intensity profile of RGB colors at  $x = 0.5\text{--}0.8$  mm.

difficult numerically to fit the two peaks or calculate their integral precisely. However, the  $\text{ARS} \sim \theta_s$  curves of the coated surfaces fit the cosine function very well (Figs 2d and S4). It is worth mentioning that structures fabricated by RIE are not defect free, which might introduce additional recombination sites when compared to defect free structures<sup>31</sup>. Nonetheless, the decrease in the surface area, and the possibility to passivate the surface by introducing alumina or  $\text{SiN}_x$  still makes the inverted pyramids fabricated by our method promising for photovoltaic applications.

In addition to being anti-reflective, some of our inverted pyramids appear “white” or greyish, which is distinctly different from the classical black or brownish silicon wafers made by RIE<sup>3,7,25,26</sup>. A clear demonstration of the special color of these nano inverted pyramids is presented by a photo of a white “DTU logo” (approx.  $3\text{ mm} \times 4\text{ mm}$ ) on a black background (Fig. 3a). The white DTU logo was fabricated using the same parameters as sample 55-10-10 on a black silicon wafer of nano spikes. The detailed fabrication procedure and parameters can be found in the experimental section and the supporting information. The SEM image in the white area clearly shows the inverted pyramids are fabricated, though a bit larger (pitch distance up to  $1\ \mu\text{m}$ ) than the structures fabricated on the polished silicon wafer (Figs 1 and 3c and S5), which might be caused by the incomplete removal of nanograss on the black silicon surface. The color of the logo clearly appears white to human eyes, as compared to the white A4 paper under the sample. The intensity profiles (extracted by ImageJ) of the RGB colors (Fig. 3d) along the red line on Fig. 3b,e) overlap well with each other, which further verifies the white color of the DTU logo<sup>32</sup>. There are some oscillations (period  $\sim 4\ \mu\text{m}$ ) on the color intensity profile, which might stem from defects of similar period in the area (Fig. S5). These defects might be caused by the inhomogeneous removal of the pre-etched nano spikes in the logo area by RIE, as no such structural irregularities are observed on samples fabricated directly from polished Si wafers (Fig. 1).

In summary, we have demonstrated a maskless one-step method to fabricate nano inverted pyramids on silicon wafers by RIE. These structures are very sensitive to the parameters used in RIE, and the total gas flow rate



can be substantial to the structure formation. The uncoated inverted pyramids have the lowest specular and total reflectance among all fabricated samples. The low total reflectance of these inverted pyramids is probably caused by a third reflection of the incoming beam by the pyramid facet. The total reflectance of the inverted pyramids is further reduced by an order of 40 after coating with a layer of  $\text{SiN}_x$ , which makes the inverted pyramid fabricated by RIE very promising for photovoltaic applications. As demonstrated by the white DTU logo, some of the inverted pyramids have a milky white color, which could be interesting in other industries. As RIE is an industrialized standardized silicon dry etching technique, our method will pave the way to large scale, cost-effective mass production of nano inverted pyramids.

## Experimental Section

**Silicon surface texturing.** All samples were textured by reactive ion etching (RIE, Pegasus D-RIE, STS, UK) on crystalline 100 mm silicon wafers (n-doped (phosphorous), resistivity 10–100  $\Omega\text{cm}$ , (100)), at different  $\text{SF}_6$  and  $\text{O}_2$  flow rates, platen power, temperature, and etching time. The white DTU logo with black background was fabricated by RIE on a pre-etched black silicon substrate coated with patterned photoresist of the DTU logo. The detailed fabrication parameters and process flow can be found in the supporting information. After RIE, all samples were cleaned by  $\text{N}_2/\text{O}_2$  plasma ( $\text{N}_2$  400 sccm,  $\text{O}_2$  70 sccm, power 1000 W) for 30 min. For the coated samples, a layer of approx. 80 nm silicon nitride ( $\text{SiN}_x$ ) was immediately deposited on the structured surface by plasma enhanced chemical vapor deposition (PECVD, SPTS, UK) after the plasma cleaning. The film thickness of  $\text{SiN}_x$  was tested by ellipsometry (Ellipsometer VASE, J.A. Woollam Co., Inc, USA) on a parallel plain wafer coated with the same parameters.

**Structure characterization.** All samples were characterized by scanning electron microscopy (SEM, Supra 40 VP, Carl Zeiss AG, Germany) at both cross-sectional and surface views. The dimension of the structures was measured by ImageJ (version 1.49s).

**Optical characterization.** The specular reflection was measured by multiple angle reflectometry (Film Tek 4000, scientific computing international, Carlsbad, USA) at normal and  $70^\circ$  incidence. The total reflectance was measured by optical spectrometer (OE65000, Ocean Optics spectrometer, USA) with an integrating sphere of  $8^\circ$  incidence (AvaSphere-50, Avantes, UK). The total reflectance measurement was calibrated by a white Lambertian scatter (SRS-99-020, LabSphere, USA). The scattering distribution of the samples was measured with an angular scatterometer, where a photodetector (New Focus Model 2032, Newport, USA) was rotated in a circular arc around the sample and the scattering intensity was evaluated in steps of  $0.1^\circ$ . A 40 mW argon-ion laser of 488 nm (60X, American Laser Corporation, USA) was used as the incident light source. The detailed description of the setup can be found in a previous publication<sup>33</sup>. Canon EOS 5D Mark II camera was used to shoot the photos of the white DTU logo on the black silicon wafer. Except for the auto white balance function, no further post processing was used on the photos. The RGB profile of the photo was extracted by ImageJ.

The silicon surface texturing, SEM characterizations, and the specular reflection measurements were carried out in a class 10–100 cleanroom (Danchip, DTU, Denmark).

## References

- Koenderink, A. F., Alu, A. & Polman, A. Nanophotonics: Shrinking light-based technology. *Science* **348**, 516–521, doi: 10.1126/science.1261243 (2015).
- Nguyen, K. N. *et al.* Study of black silicon obtained by cryogenic plasma etching: approach to achieve the hot spot of a thermoelectric energy harvester. *Microsystem Technologies-Micro-and Nanosystems-Information Storage and Processing Systems* **18**, 1807–1814, doi: 10.1007/s00542-012-1486-0 (2012).
- Nguyen, K. N., Basset, P., Marty, F., Leprince-Wang, Y. & Bourouina, T. On the optical and morphological properties of microstructured Black Silicon obtained by cryogenic-enhanced plasma reactive ion etching. *Journal of Applied Physics* **113**, doi: 10.1063/1.4805024 (2013).
- Campbell, P. & Green, M. A. High performance light trapping textures for monocrystalline silicon solar cells. *Solar Energy Materials and Solar Cells* **65**, 369–375, doi: 10.1016/s0927-0248(00)00115-x (2001).
- Liu, X. G. *et al.* Black silicon: fabrication methods, properties and solar energy applications. *Energy & Environmental Science* **7**, 3223–3263, doi: 10.1039/c4ee01152j (2014).
- Ingenito, A., Isabella, O. & Zeman, M. Nano-cones on micro-pyramids: modulated surface textures for maximal spectral response and high-efficiency solar cells. *Progress in Photovoltaics* **23**, 1649–1659, doi: 10.1002/pip.2606 (2015).
- Jansen, H., Deboer, M., Burger, J., Legtenberg, R. & Elwenspoek, M. The black silicon method. 2 the effect of mask material and loading on the reactive ion etching of deep silicon trenches. *Microelectronic Engineering* **27**, 475–480, doi: 10.1016/0167-9317(94)00149-o (1995).
- Dagostino, R. & Flamm, D. L. Plasma-etching of si and  $\text{SiO}_2$  in  $\text{SF}_6$ - $\text{O}_2$  mixtures. *Journal of Applied Physics* **52**, 162–167, doi: 10.1063/1.328468 (1981).
- Cho, S. J., An, T., Kim, J. Y., Sung, J. & Lim, G. Superhydrophobic nanostructured silicon surfaces with controllable broadband reflectance. *Chemical Communications* **47**, 6108–6110, doi: 10.1039/c1cc11615k (2011).
- Christiansen, A. B. *et al.* Black metal thin films by deposition on dielectric antireflective moth-eye nanostructures. *Scientific Reports* **5**, doi: 10.1038/srep10563 (2015).
- Yue, Z. H., Shen, H. L. & Jiang, Y. Antireflective nanostructures fabricated by reactive ion etching method on pyramid-structured silicon surface. *Applied Surface Science* **271**, 402–406, doi: 10.1016/j.apsusc.2013.01.216 (2013).
- Branham, M. S. *et al.* 15.7% Efficient 10- $\mu\text{m}$ -Thick Crystalline Silicon Solar Cells Using Periodic Nanostructures. *Advanced Materials* **27**, 2182–+, doi: 10.1002/adma.201405511 (2015).
- Mavrokefalos, A., Han, S. E., Yerci, S., Branham, M. S. & Chen, G. Efficient Light Trapping in Inverted Nanopyramid Thin Crystalline Silicon Membranes for Solar Cell Applications. *Nano Letters* **12**, 2792–2796, doi: 10.1021/nl2045777 (2012).
- Savin, H. *et al.* Black silicon solar cells with interdigitated back-contacts achieve 22.1% efficiency. *Nature Nanotechnology* **10**, 624–+, doi: 10.1038/nnano.2015.89 (2015).
- Han, S. E. & Chen, G. Optical Absorption Enhancement in Silicon Nanohole Arrays for Solar Photovoltaics. *Nano Letters* **10**, 1012–1015, doi: 10.1021/nl904187m (2010).

16. Sivasubramaniam, S. & Alkai, M. M. Inverted nanopillar texturing for silicon solar cells using interference lithography. *Microelectronic Engineering* **119**, 146–150, doi: 10.1016/j.mee.2014.04.004 (2014).
17. Chen, H. Y. *et al.* Enhanced photovoltaic performance of inverted pyramid-based nanostructured black-silicon solar cells passivated by an atomic-layer-deposited Al<sub>2</sub>O<sub>3</sub> layer. *Nanoscale* **7**, 15142–15148, doi: 10.1039/c5nr03353e (2015).
18. Kumar, K., Khalatpour, A., Nogami, J., Kherani, N. P. & Ieee. Optimizing Inverted Pyramidal Grating Texture for Maximum Photoabsorption in Thick to Thin Crystalline Silicon Photovoltaics. *Ieee 40th Photovoltaic Specialist Conference (Pvsc)*, 605–607 (2014).
19. Schuster, C. S., Bozzola, A., Andreani, L. C. & Krauss, T. F. How to assess light trapping structures versus a Lambertian Scatterer for solar cells? *Optics Express* **22**, A542–A551, doi: 10.1364/oe.22.00a542 (2014).
20. Wang, Y. *et al.* Maskless inverted pyramid texturization of silicon. *Scientific Reports* **5**, doi: 10.1038/srep10843 (2015).
21. Trompoukis, C. *et al.* Disordered nanostructures by hole-mask colloidal lithography for advanced light trapping in silicon solar cells. *Optics Express* **24**, A191–A201, doi: 10.1364/oe.24.00a191 (2016).
22. Gao, X. F. *et al.* The dry-style antifogging properties of mosquito compound eyes and artificial analogues prepared by soft lithography. *Advanced Materials* **19**, 2213–+, doi: 10.1002/adma.200601946 (2007).
23. Schneider, L., Laustsen, M., Mandsberg, N. & Taboryski, R. The Influence of Structure Heights and Opening Angles of Micro- and Nanocones on the Macroscopic Surface Wetting Properties. *Scientific Reports* **6**, doi: 10.1038/srep21400 (2016).
24. Sainiemi, L. *et al.* Non-Reflecting Silicon and Polymer Surfaces by Plasma Etching and Replication. *Advanced Materials* **23**, 122–+, doi: 10.1002/adma.201001810 (2011).
25. Saab, D. A., Basset, P., Pierotti, M. J., Trawick, M. L. & Angelescu, D. E. Static and Dynamic Aspects of Black Silicon Formation. *Physical Review Letters* **113**, doi: 10.1103/PhysRevLett.113.265502 (2014).
26. Jansen, H. V., de Boer, M. J., Unnikrishnan, S., Louwse, M. C. & Elwenspoek, M. C. Black silicon method X: a review on high speed and selective plasma etching of silicon with profile control: an in-depth comparison between Bosch and cryostat DRIE processes as a roadmap to next generation equipment. *Journal of Micromechanics and Microengineering* **19**, doi: 10.1088/0960-1317/19/3/033001 (2009).
27. Gao, P. Q. *et al.* Large-Area Nanosphere Self-Assembly by a Micro-Propulsive Injection Method for High Throughput Periodic Surface Nanotexturing. *Nano Letters* **15**, 4591–4598, doi: 10.1021/acs.nanolett.5b01202 (2015).
28. Lin, Q. F. *et al.* Inverted Nanocone-Based Thin Film Photovoltaics with Omnidirectionally Enhanced Performance. *Acs Nano* **8**, 6484–6490, doi: 10.1021/nn5023878 (2014).
29. Zhao, J. H., Wang, A. H., Altermatt, P. P., Wenham, S. R. & Green, M. A. 24% efficient PERL silicon solar cell: Recent improvements in high efficiency silicon cell research. *Solar Energy Materials and Solar Cells* **41-2**, 87–99, doi: 10.1016/0927-0248(95)00117-4 (1996).
30. Narasimhan, V. K., Hymel, T. M., Lai, R. A. & Cui, Y. Hybrid Metal-Semiconductor Nano structure for Ultrahigh Optical Absorption and Low Electrical Resistance at Optoelectronic Interfaces. *Acs Nano* **9**, 10590–10597, doi: 10.1021/acs.nano.5b04034 (2015).
31. Nakakubo, Y., Eriguchi, K. & Ono, K. Characterization of Plasma Process-Induced Latent Defects in Surface and Interface Layer of Si Substrate. *Ecs Journal of Solid State Science and Technology* **4**, N5077–N5083, doi: 10.1149/2.0121506jss (2015).
32. Klein, A. G. *Industrial Color Physics*. 1. edn, Vol. 154 p XIV, 509 (Springer-Verlag New York, 2010).
33. Feidenhans, N. A. I. *et al.* Comparison of optical methods for surface roughness characterization. *Measurement Science & Technology* **26**, doi: 10.1088/0957-0233/26/8/085208 (2015).

## Acknowledgements

The authors thank Mr. Suhith Hemanth for providing the photomask; Dr. Carsten Dam-Hansen for sharing the equipment; Mr. Nikolaj Kofoed Mandsberg for providing Matlab scripts; and Dr. Holger Schneider for inspiring discussion and valuable suggestions. This work was supported by EU's 7 Frame Work Program, through the FoF. NMP.2012-7 project "Plast4Future", with grant agreement number 314345.

## Author Contributions

L.S. and R.J.T. conceived the project. L.S. and A.T. fabricated the samples. N.A.F. made the optical characterization of the samples. L.S. and N.A.F. made the data analysis. L.S. and R.J.T. wrote the manuscript with comments from all authors. Approval of the final version was given by all authors.

## Additional Information

**Supplementary information** accompanies this paper at <http://www.nature.com/srep>

**Competing financial interests:** The authors declare no competing financial interests.

**How to cite this article:** Schneider, L. *et al.* One-step Maskless Fabrication and Optical Characterization of Silicon Surfaces with Antireflective Properties and a White Color Appearance. *Sci. Rep.* **6**, 35183; doi: 10.1038/srep35183 (2016).



This work is licensed under a Creative Commons Attribution 4.0 International License. The images or other third party material in this article are included in the article's Creative Commons license, unless indicated otherwise in the credit line; if the material is not included under the Creative Commons license, users will need to obtain permission from the license holder to reproduce the material. To view a copy of this license, visit <http://creativecommons.org/licenses/by/4.0/>

© The Author(s) 2016